Lecture 15. Numerical Modeling

Most atmospheric models use partial differential equations which are solved numerically. A computational grid and numerical method selected to solve the equations are based on the following criteria

- *Accuracy*, which for a simple problem can be estimated by comparing the numerical solution with its analytical counterpart;
- *Stability*, which often imposes a restriction on the time step;
- *Transportivity*, which requires that any perturbation is advected downwind;
- *Locality*, such that the solution of the advection problem at a given point is not significantly influenced by the field far from that point;
- *Conservation*, which requires that no gain nor loss of mass occurs during the transport;
- *Monotonicity* (shape preserving), through which the occurrence of new extrema is prohibited; these extrema (noise) are characterized by undershoots and overshoots near regions of strong gradients;
- *Efficiency*, such that the computer time consumed is not prohibitive, and the storage requirement does not exceed computer capacity

1 Numerical Grid

A grid is defined as a set of cells created by edges joining pairs of vertices defined in a discretization. The most common form of cells is rectangular, but triangular is also used for specific applications.

RECTANGULAR GRID

The most commonly used discretization in Earth system science is logically rectangular with spherical coordinates. However, it necessitates filtering of the variables at the pole due to their singularity. The filter is limiting the parallelization and is not always conservative, such that more specialized grids such as the tripolar or cubed-sphere grids are preferably used on massively parallel computers.
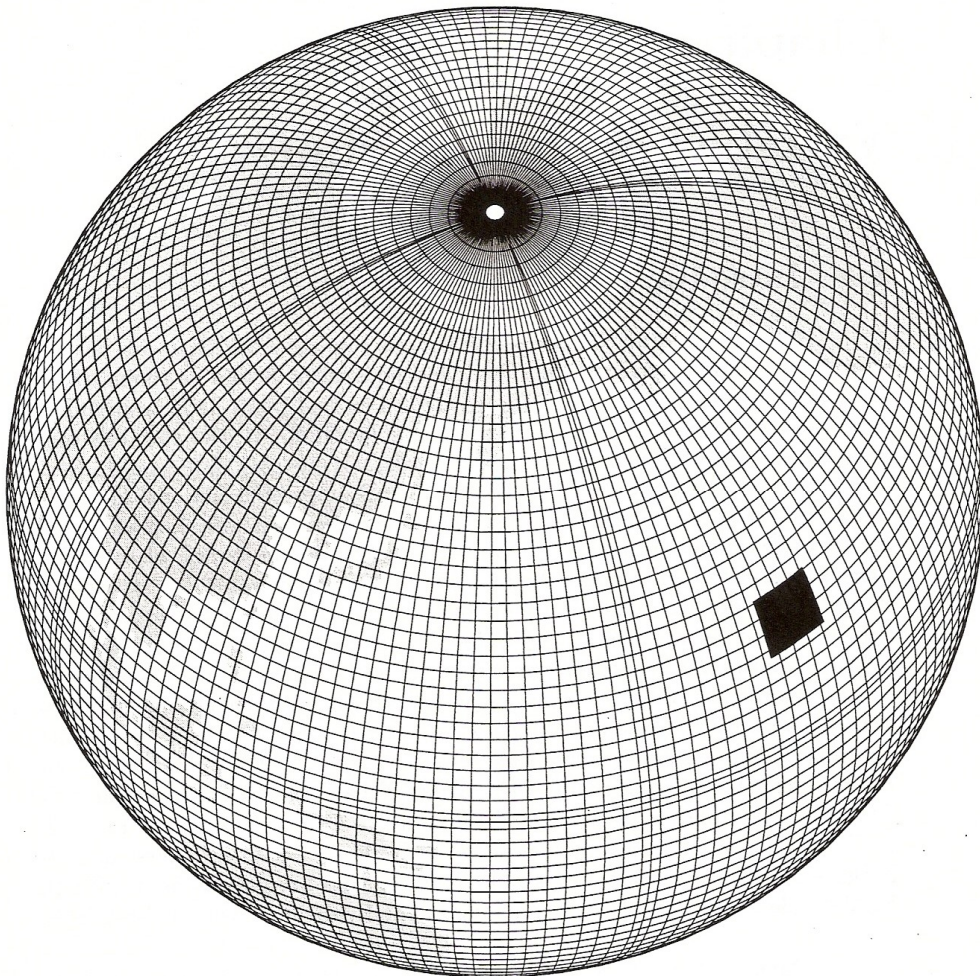

Figure 1 Global Cartesiand grid used by ECMWF re-analysis with a 2.5x2.5 degree spacing. Singularity at the poles require polar capping
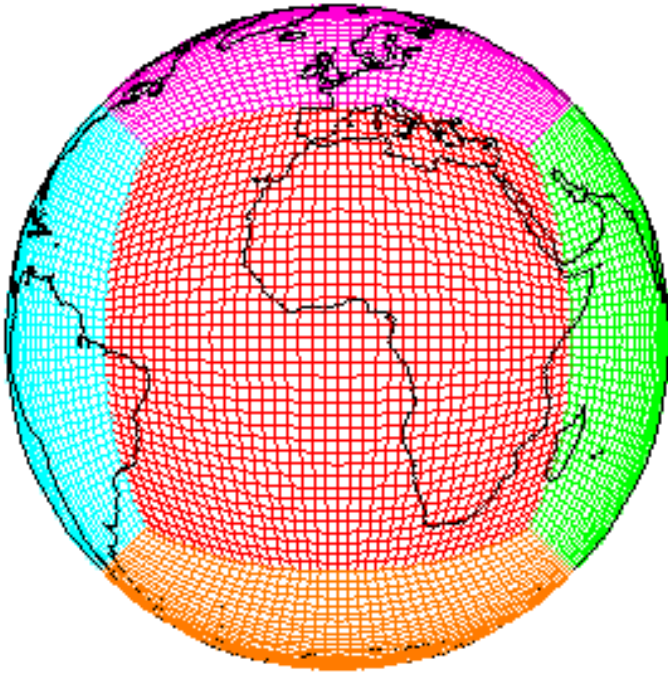
Figure 2 Cube-sphere grid, projecting the sphere onto the 6 faces of a cube. Polar singularities are avoided, at the expense of some grid distorsion near the cube's vertices.
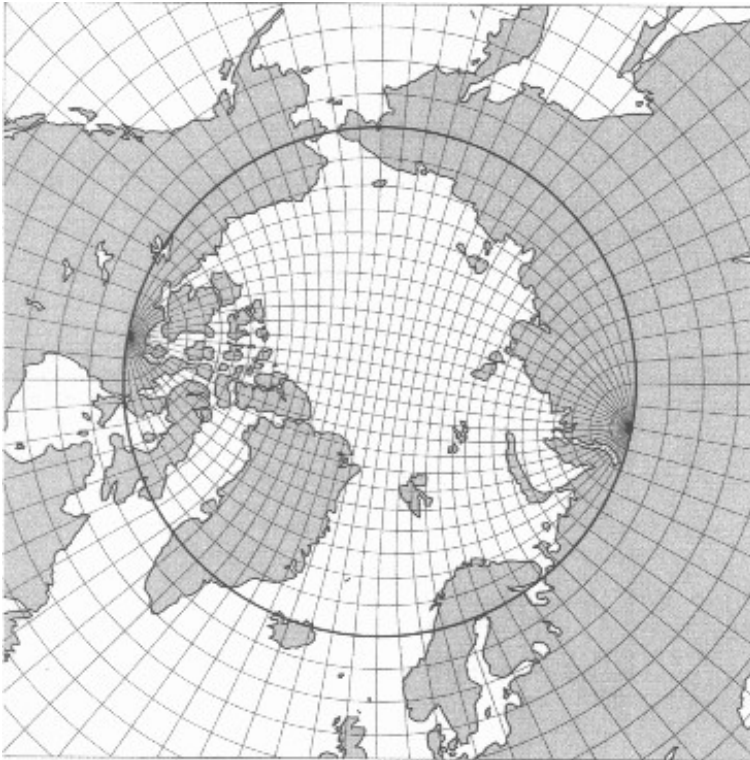

Figure 4 Tripolar grid, often used in ocean modeling. Polar singularities are placed over land and excluded from the simulation.

TRIANGULAR GRID

Triangular discretizations are increasingly voguish in the field. A structured triangular discretization of an icosahedral projection is a popular new approach resulting in a geodesic grid. An example of a structured triangular grid is shown in the Figure below. The grid is generated by recursive division of the 20 triangular faces of an icosahedron.
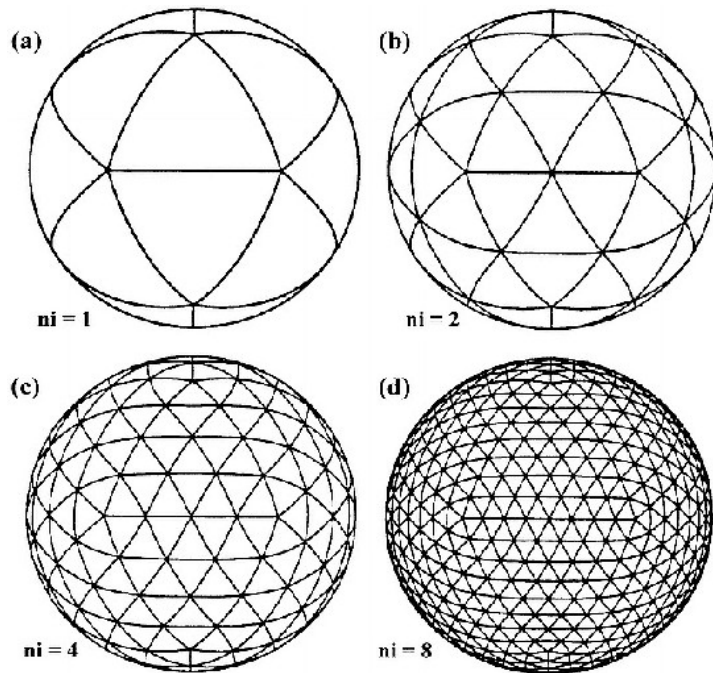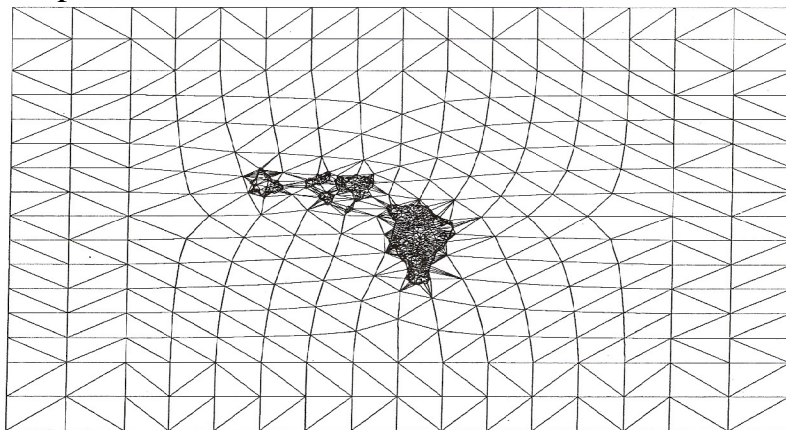

Figure 3 A structured triangular discretization of the sphere. Note that all vertices at any truncation level ni are also vertices at any higher level of truncation.

UNSTRUCTURED GRID

Numerically generated unstructured triangular discretizations are often used over complex terrain.

STAGGERING GRID

Algorithms place quantities at different locations within a grid cell ("staggering"). The staggering of the grids is related with the computational stability of various numerical schemes. The Arakawa grids show different ways to represent velocities and masses on grids
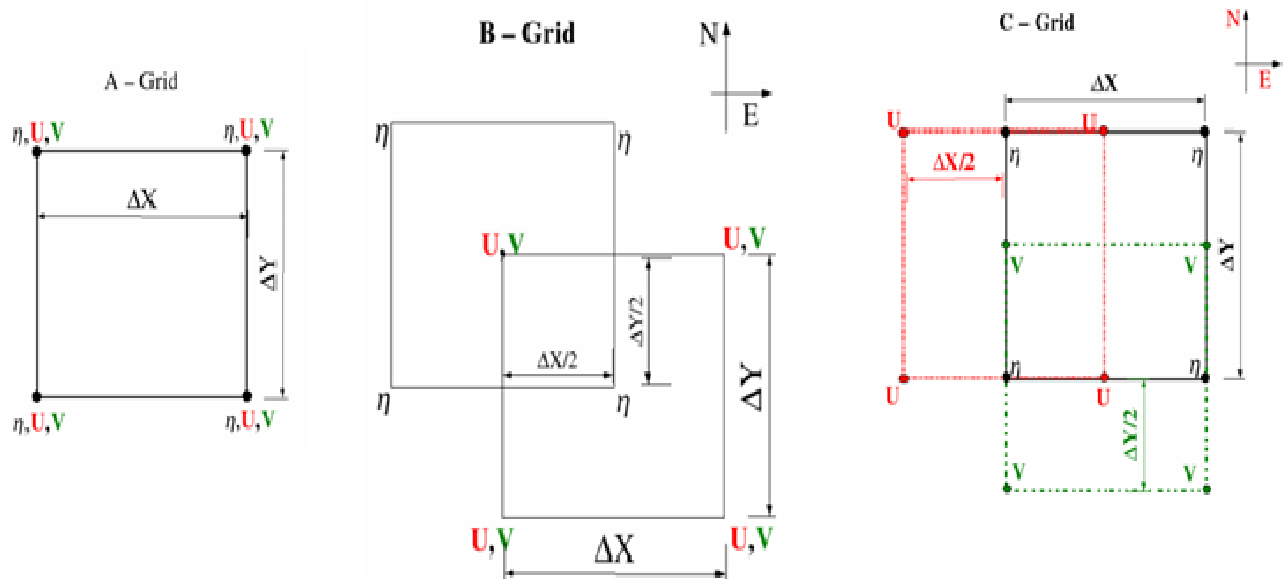
GRID REFINMENT

A refined grid is usually a fine grid overlying a coarse grid, with some refinement ratio between their grid spacing. The vertices on the coarse grid are also vertices on the fine grid.

For nested grids, the grids must be aligned with the model coordinates, and the mesh refinement ratio of the temporal and spatial grid increments is common for all meshes. The interactions between meshes can be 1-way (coarse to fine) or 2-way (coarse-fine-coarse).

The most important element for any mesh refinement method is an accurate and efficient interpolation procedure.
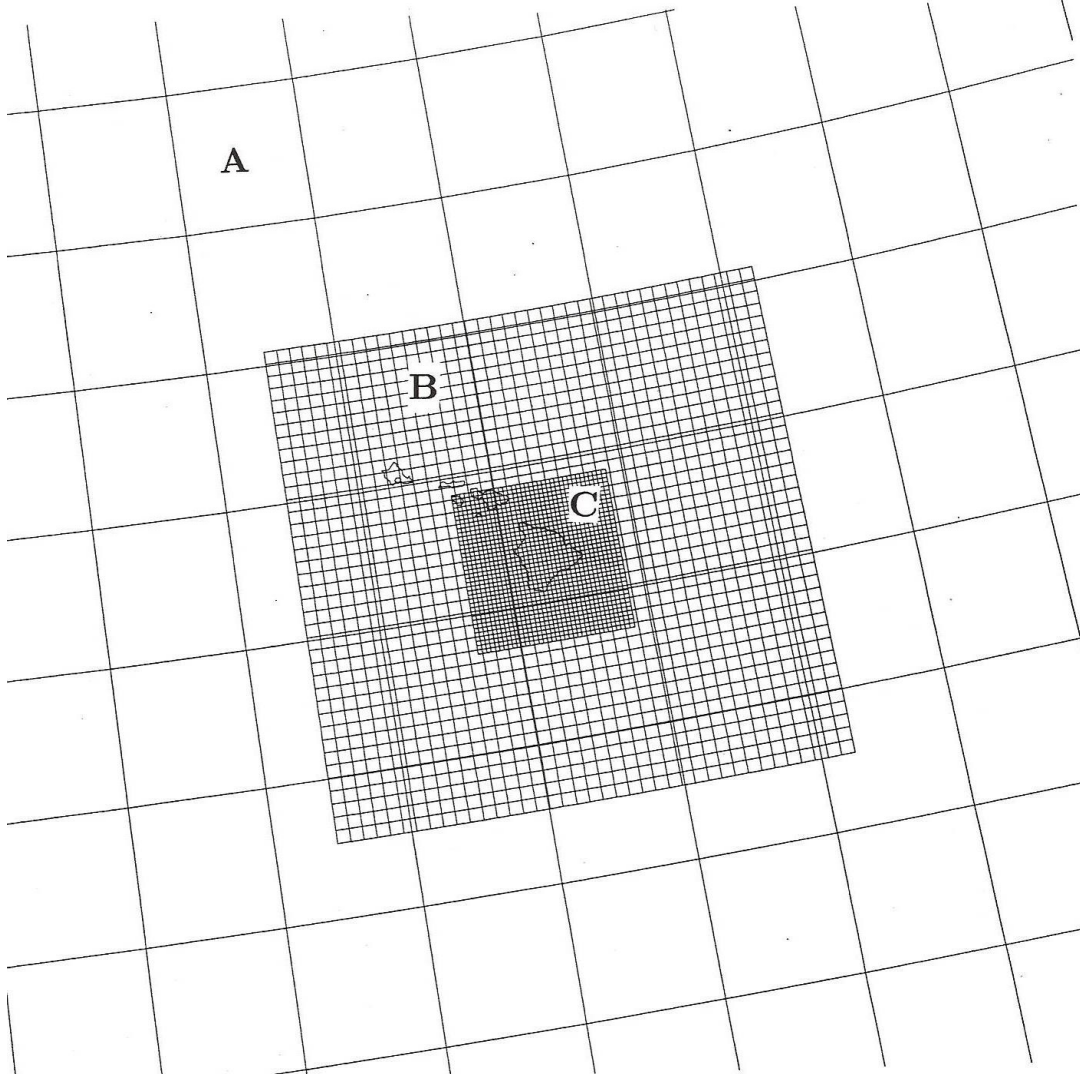
Figure 3. Nested grids over Hawaii: A. Coarse global 2.5x2.5 grid; B. Finer grid (27x27 km) over the Hawaii islands; C. Very fine resolution (9x9 km) over Hawaii big island.

In a 2-way interactions, the solution from the fine grid feeds back into the coarse grid. Without smoothing or averaging, the solution on the coarse grid will appear noisy. The Shapiro filter is generally applied. The algorithm of the Shapiro filter applied to the variable ψ is given by

$$\overline{\psi}(i,j) = \psi(i,j) + \frac{\nu}{2}(1-\nu)[\psi(i+1,j) + \psi(i-1,j) + \psi(i,j+1) + \psi(i,j-1) + 4\psi(i,j)]$$

$$+ \frac{\nu^2}{4}[\psi(i+1,j+1) + \psi(i+1,j-1) + \psi(i-1,j+1) + \psi(i-1,j-1) - 4\psi(i,j)]$$

Where $\nu = 0.5$ for the nine point averager.

EXCHANGE GRID

Given two grids, an exchange grid is the set of cells defined by the union of all the vertices of the two parent grids.
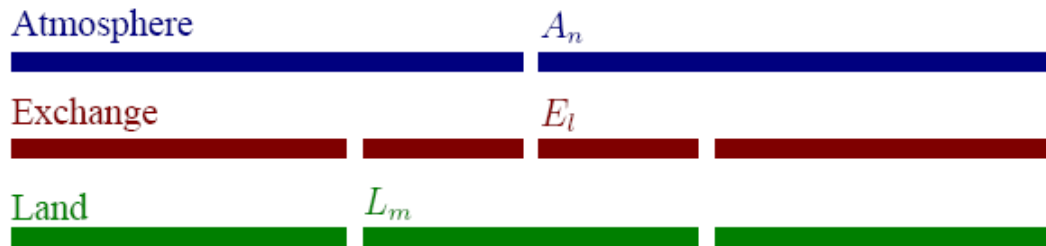
Each exchange grid cell E_l can be uniquely associated with exactly one cell on each parent grid, and fractional areas with respect to the parent grid cells. Quantities being transferred from one parent grid to the other are first interpolated onto the exchange grid using one set of fractional areas; and then averaged onto the receiving grid using the other set of fractional areas. If a particular moment of the exchanged quantity is required to be conserved, consistent moment-conserving interpolation and averaging functions of the fractional area may be employed. This may require not only the cell-average of the quantity (zeroth-order moment) but also higher-order moments to be transferred across the exchange grid.

MASK

A complication arises when one of the surfaces is partitioned into complementary components: in Earth system models, a typical example is that of an ocean and land surface that together tile the area under the atmosphere. Conservative exchange between three components may then be required: quantities like CO2 have reservoirs in all three media, with the total carbon inventory being conserved.
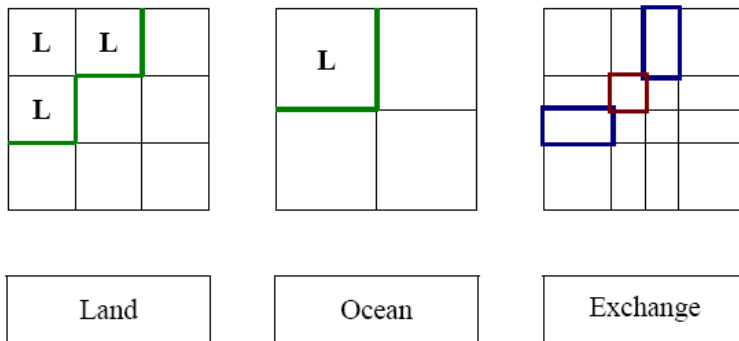
The Figure above shows such an instance, with an atmosphere-land grid and an ocean grid of different resolution. The green line in the first two frames shows the land-sea mask as discretized on the two grids, with the cells marked L belonging to the land. Due to the differing resolution, certain exchange grid cells have ambiguous status: the two blue cells are claimed by both land and ocean, while the orphan red cell is claimed by neither.

Cells of ambiguous status are resolved by adopting some ownership convention. For example, in the exchange grid, the land model is modified as needed: the land grid cells are quite independent of each other and amenable to such transformations. Cells are added to the land grid until there are no orphan "red" cells left on the exchange grid, then get rid of the "blue" cells by clipping the fractional areas on the land side.

GRID TILING

A further complication arises when we consider tiles within parent grid cells. Tiles are a refinement within physical grid cells, where a quantity is partitioned among "bins" each owning a fraction of it. Tiles within a grid cell do not have independent physical locations, only their associated fraction. Examples include different vegetation types within a single land grid cell, which may have different temperature or moisture retention properties, or partitions of different ice thickness representing fractional ice coverage within a grid cell.

IMPLICIT COUPLING

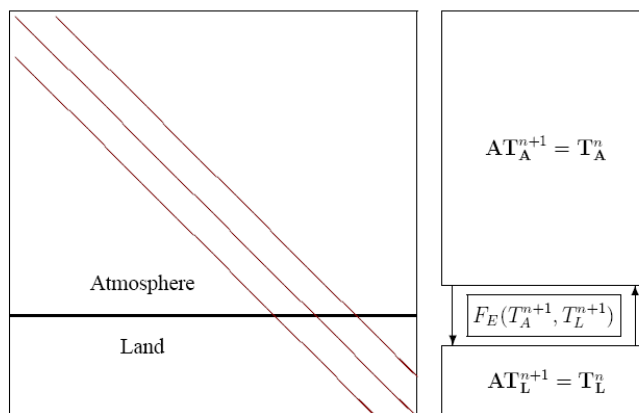Fluxes at the surface often need to be treated using an implicit timestep.

$$AT_A^{n+1} = T_A^n$$

$$F_E(T_A^{n+1}, T_L^{n+1})$$

$$AT_L^{n+1} = T_L^n$$

Figure. Tridiagonal inversion across multiple components and an exchange grid. The tmospheric and land temperatures T_A and T_L are part of an implicit diffusion equation, coupled by the implicit surface flux on the exchange grid, $F_E(T_{n+1A}\,;\,T_{n+1L})$.

The general procedure for solving such trid-diagonal matrix is to split into separate up and down steps. In GFDL model there is a first sweep down the atmosphere ("`atmosphere_down`" step) and then handed off to the exchange grid, where fluxes are computed. The land or ocean surface models recover the values from the exchange grid and continue the calculation and return values to the exchange grid. The computation is then completed in the up-sweep of the atmosphere.

PARALLELIZATION

In general, not only are the parent grids physically independent, they are also parallelized independently. Thus, for any exchange grid, the parent cells may be on different processors. A choice has to be made either:
1. to inherit the parallel decomposition from one of the parent grids (thereby eliminating communication for one of the data exchanges); or
2. to assign an independent decomposition to the exchange grid, which may provide better load balance.

In the GFDL exchange grid design, the first choice has been selected.

2 Numerical methods

1.1.   Numerical Method for advection

To simplify, we consider 1D advection equation

$$\frac{\partial \psi}{\partial t} + u \frac{\partial \psi}{\partial x} = 0$$

1.1.1.   Eulerian algorithm

Spatial grid points are fixed and flux of air mass passing through them is computed. The general limitation comes from the Courant-Friedricks-Lewy (CFL) stability criterion

$$\frac{|u|\Delta t}{\Delta x} \leq C$$

where C is a constant of order unity.

| Scheme	Algebraic Form	Stability	Accuracy
Euler forward	$\Psi_j^{n+1} = \Psi_j^n + \frac{u\Delta t}{2\Delta x}\left(\Psi_{j-1}^n - \Psi_{j+1}^n\right)$	Unstable	$O\left(\Delta t, \Delta x^2\right)$
Upwind	$\Psi_j^{n+1} = \Psi_j^n + \frac{u\Delta t}{\Delta x}\left(\Psi_{j-1}^n - \Psi_j^n\right)$	$\frac{u\Delta t}{\Delta x} \leq 1$	$O\left(\Delta t, \Delta x\right)$
Leapfrog	$\Psi_j^{n+1} = \Psi_j^{n-1} + \frac{u\Delta t}{\Delta x}\left(\Psi_{j-1}^n - \Psi_{j+1}^n\right)$	$\frac{u\Delta t}{\Delta x} \leq 1$	$O\left(\Delta t^2, \Delta x^2\right)$
Lax-Wendroff	$\Psi_j^{n+1} = \Psi_j^n + \frac{u\Delta t}{2\Delta x}\left(\Psi_{j-1}^n - \Psi_{j+1}^n\right) +$ $\frac{1}{2}\left(\frac{u\Delta t}{\Delta x}\right)^2\left(\Psi_{j-1}^n - 2\Psi_j^n + \Psi_{j+1}^n\right)$	$\frac{u\Delta t}{\Delta x} \leq 1$	$O\left(\Delta t^2, \Delta x^2\right)$
Crank-Nicholson	$-\frac{u\Delta t}{2\Delta x}\Psi_{j-1}^{n+1} + 2\Psi_j^{n+1} + \frac{u\Delta t}{2\Delta x}\Psi_{j+1}^{n+1} =$ $\frac{u\Delta t}{2\Delta x}\left(\Psi_{j-1}^n - \Psi_{j+1}^n\right)$	Stable	$O\left(\Delta t^2, \Delta x^2\right)$
Chapeau (FEM)	$\left(\frac{1}{3} - \frac{u\Delta t}{2\Delta x}\right)\Psi_{j-1}^{n+1} + \frac{4}{3}\Psi_j^{n+1} + \left(\frac{1}{3} + \frac{u\Delta t}{2\Delta x}\right)\Psi_{j+1}^{n+1} =$ $\left(+\frac{1}{3} - \frac{u\Delta t}{2\Delta x}\right)\Psi_{j-1}^n + \frac{4}{3}\Psi_j^n + \left(\frac{1}{3} - \frac{u\Delta t}{2\Delta x}\right)\Psi_{j+1}^n$	Stable	$O\left(\Delta t^2, \Delta x^4\right)$

1.1.2. Semi-lagrangian algorithm

In semi-lagrangian formulation, the solution on prescribed grid points is derived at each time step on the basis of a Lagrangian backward calculation. The initial position x_i^n of the grid point i at time t^n, which after one time Δt step arrives at the mesh point x_i^{n+1}, is calculated by

$$x_i^n = x_i^{n+1} - \int_{t^n}^{t^{n+1}} u_i\, dt$$

In general x_i^n does not coincide with x_i^{n+1}, so that the velocity u_i has to be estimated by interpolation (NB. u_i should be interpolated in time and space).
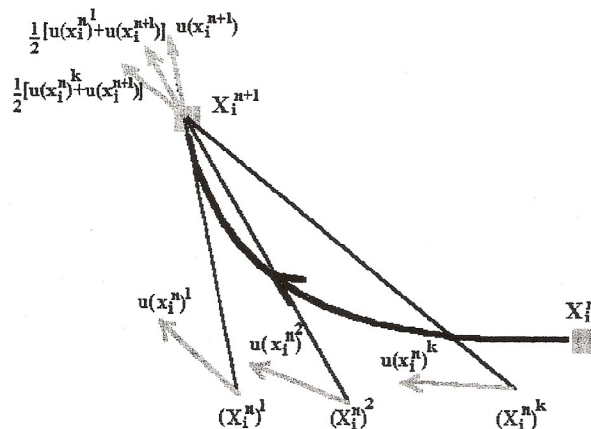
The success of the method (accuracy, monotonicity, shape preserving) is greatly dependent on the interpolation scheme used.
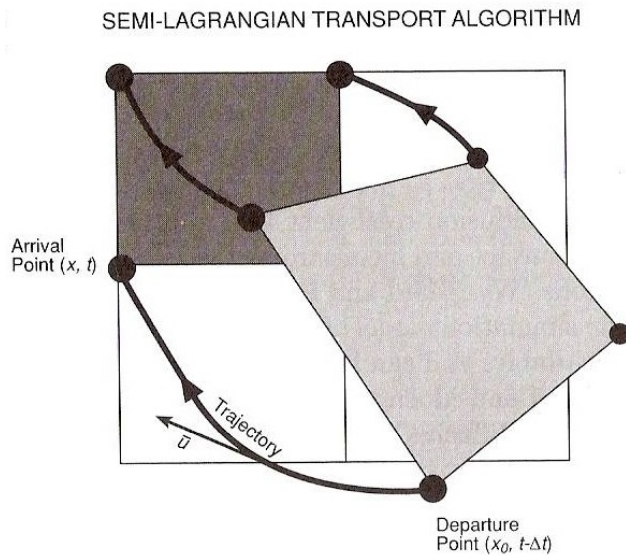
An algorithm to calculate the back-trajectory position is:

$$(x_i^n)^k = x_i^{n+1} - \Delta t \left(\frac{u_i((x_j^n)^{k-1}) + u_i(x_j^{n+1})}{2} \right)$$

where k is the iteration level. The maximum number of iteration depends on how far apart are the calculation position $(x_i^n)^k$ and $(x_i^n)^{k-1}$


1.1.3.   Lagrangian

In the Lagrangian schemes, distinct air parcels, in which the tracers are assumed to be homogenously mixed, are followed as they are displaced. Lagrangian schemes are simple but the accumulation of errors in determining parcel location is too large for global models.

1.1.4. Algorithm Evaluation

The performances of numerical schemes are compared with simple tests. For example, the advection at constant speed of a triangle shows that linear schemes are diffusive and does not preserve the shape, while high order schemes are shape preserving but produce overshooting and undershooting (negative values!).
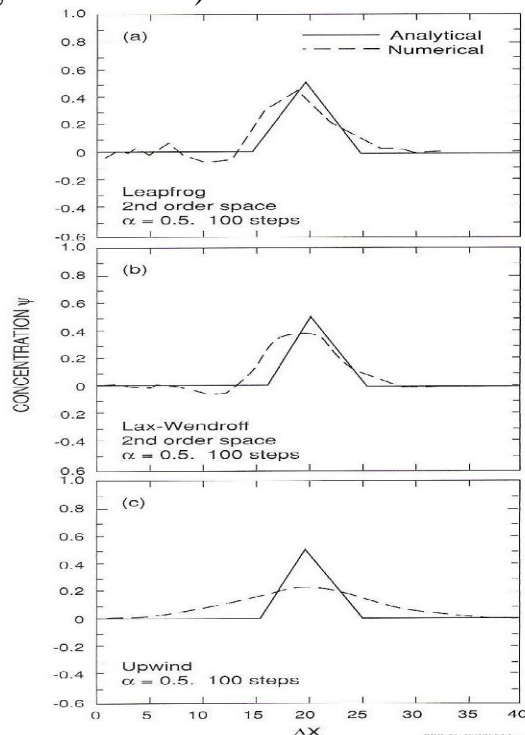
1.1.5. Mass Fixer

Negative tracer values can be generated by several different terms. The advection of tracers using centered differencing schemes may be the largest contributor to negative tracer. Also the use of polar filtering with the centered difference advection scheme is a very large contributor in high latitudes. Another less obvious source of negative tracer is higher-order horizontal mixing. The second-order smoothing operator does not create negative tracer, but the fourth-order or higher schemes can create negative tracer when there are very sharp gradients.

With semi-Lagrangian finite-volume advection schemes the source of negative tracer is limited to truncation errors.

Negative concentration should be corrected with a mass conservative and non-diffusive scheme. Diffusive schemes (e.g. Shapiro filtering) are conservative but are not shape preserving. Filling schemes borrow from the nearest grid points in the vertical and horizontal in a way that conserves the global tracer mass.

1.2.   Numerical Method for diffusion

The 1D diffusion transport equation of a ψ is given by

$$\frac{\partial \psi}{\partial t} = \frac{\partial}{\partial x}\left(K\frac{\partial \psi}{\partial x}\right)$$

where K is the so-called diffusion coefficient. There are several algorithms available to solve this equation. The explicit scheme is stable only if

$$\frac{2K\Delta t}{(\Delta x)^2} \leq 1$$

While Crank-Nicholson, Chapeau, and fully implicit are unconditionally stable. These last three schemes result in tridiagonal matrix.

Scheme	Algebraic Form	Stability	Accuracy
Euler forward	$\Psi_j^{n+1} = \Psi_j^n + \frac{K\Delta t}{\Delta x^2}\left[\Psi_{j-1}^n - 2\Psi_j + \Psi_{j+1}^n\right]$	$\frac{K\Delta t}{\Delta x^2} \leq 0.5$	$O\left(\Delta t, \Delta x^2\right)$
Crank-Nicholson	$-\frac{K\Delta t}{2\Delta x^2}\Psi_{j-1}^{n+1} + \left(1 + \frac{K\Delta t}{\Delta x^2}\right)\Psi_j^{n+1} - \frac{K\Delta t}{2\Delta x^2}\Psi_{j+1}^{n+1} =$		
	$\frac{K\Delta t}{2\Delta x^2}\Psi_{j-1}^n + \left(1 - \frac{K\Delta t}{\Delta x^2}\right)\Psi_j^n + \frac{K\Delta t}{2\Delta x^2}\Psi_{j+1}^n$	Stable	$O\left(\Delta t, \Delta x^2\right)$
Fully Implicit	$-\frac{K\Delta t}{2\Delta x^2}\Psi_{j-1}^{n+1} + \left(1 + \frac{K\Delta t}{\Delta x^2}\right)\Psi_j^{n+1}$		
	$-\frac{K\Delta t}{2\Delta x^2}\Psi_j^{n+1} = \Psi_j^n$	Stable	$O\left(\Delta t, \Delta x^2\right)$
Chapeau (FEM)	$\left(\frac{1}{6} - \frac{K\Delta t}{2\Delta x^2}\right)\Psi_{j-1}^{n+1} + \left(\frac{2}{3} + \frac{K\Delta t}{\Delta x^2}\right)\Psi_j^{n+1}$		
	$+ \left(\frac{1}{6} - \frac{K\Delta t}{2\Delta x^2}\right)\Psi_{j+1}^{n+1} = \left(\frac{1}{6} + \frac{K\Delta t}{2\Delta x^2}\right)\Psi_{j-1}^n$		
	$+ \left(\frac{2}{3} - \frac{K\Delta t}{\Delta x^2}\right)\Psi_j^n + \left(\frac{1}{6} - \frac{K\Delta t}{2\Delta x^2}\right)\Psi_{j+1}^n$	Stable	$O\left(\Delta t, \Delta x^2\right)$
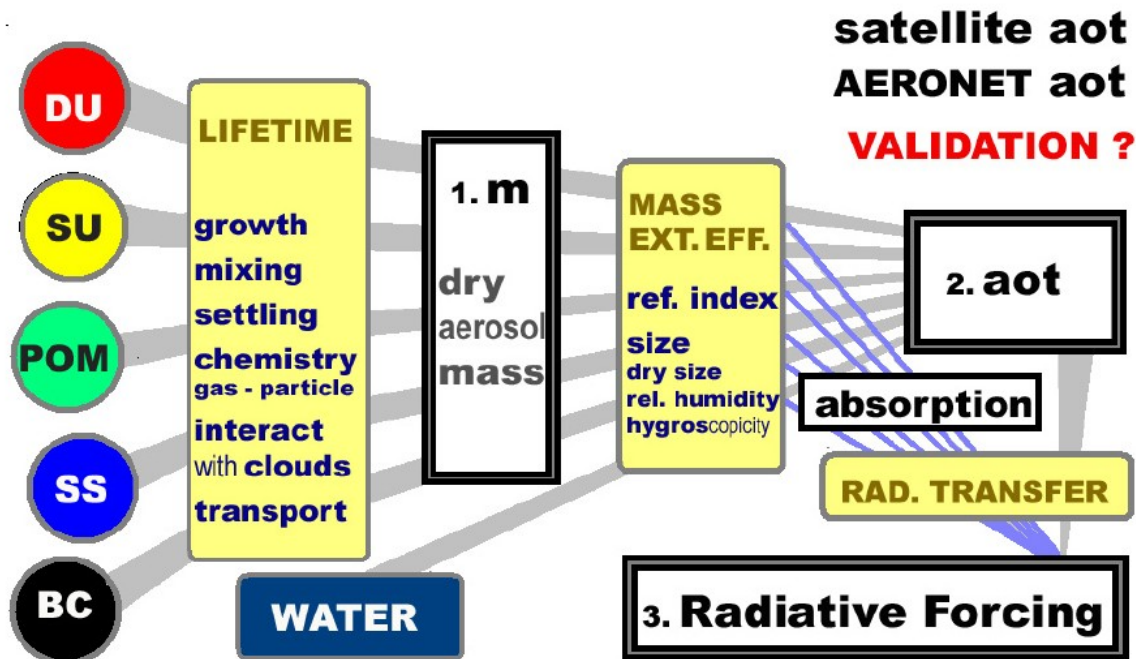
1. Prepare input files of anthropogenic aerosol emission

Table 1. AeroCom common (natural) emissions.

	time resolution	aero type*	injection altitude	size ln r_m[μm]	size ln σ	r_{eff} [μm]	flux [Tg/yr] AeroCom	flux [Tg/yr] IPCC-TAR
dust	daily	DU	surface	.650 [C]	2.0[C]	2.10	1678	2150 +/−50%
sea-salt	daily	SS	surface	.740[C]	2.0[C]	2.50	7925	3340 +/−80%
DMS	daily	S	surface	.040	1.8	.095	18.2	25 +/−60%
volcanic, explosive	yearly	S [+]	(V_T+500 m)– (V_T+1500 m)	.040 50% .015 50%	1.8	.059	2.0	
volcanic, continuous	yearly	S [+]	(.67 *V_T)– (1.0 *V_T)	.040 50% .015 50%	1.8	.059	12.6	9.3 [4–20] expl.+cont.
SOA	monthly	POM	surface				19.1	[12–70] [K]

* DU-dust, SS-sea-salt, S-sulfur (=0.50×SO_2, or 0.33×SO_4), POM-particulate org matter (=1.40×organic carbon)
[+] only 2.5% of sulfur (S) should be emitted as particulate SO_4, most sulfur (S) is emitted as gaseous SO_4
[C] log-normal size-distribution parameters of the coarse size mode
[K] based on a recent review by Kanakidou et al. (2005)

Table 2. AeroCom anthropogenically (full molecular mass) emissions for the year 2000.

type	data source	time resolution	aero type	injection altitude	size (ln) $r_m[\mu m]$	size σ	r_{eff} [μm]	flux[Tg/yr] AeroCom	flux [Tg/yr] IPCC-TAR
wild-fire	GFED	monthly	BC	6 layers [H]	.040	1.8	.095	3.1	5.7 [5–9]
	GFED	monthly	POM	6 layers [H]	.040	1.8	.095	34.7	54 [45–80]
	GFED	monthly	S [+]	6 layers [H]	.040	1.8	.095	2.1	2.2 [1–6]
biofuel	SPEW	yearly	BC	surface	.040	1.8	.095	1.6	in wild fire
	SPEW	yearly	POM	surface	.040	1.8	.095	9.1	
domestic	IIASA	yearly	S [+]	surface	.015	1.8	.036	9.6	11.4[B]
fossilfuel	SPEW	yearly	BC	surface	.015	1.8	.036	3.0	6.6 [6–8]
	SPEW	yearly	POM	surface	.015	1.8	.036	3.2 (+19.1)	28 [10–30][A]
roads	IIASA	yearly	S [+]	surface	.015	1.8	.036	1.9	3.6[B]
shipping	EDGAR	yearly	S [+]	surface	.500	2.0	1.66	7.8	7.3[B]
off-road	IIASA	yearly	S [+]	surface	.015	1.8	.036	1.6	1.9[B]
industry	IIASA	yearly	S [+]	100–300 m	.500	2.0	1.66	39.2	67.5[B]
power-pl.	IIASA	yearly	S [+]	100–300 m	.500	2.0	1.66	48.4	53.6[B]

* S-sulfur (=0.50× SO_4, or 0.33× SO_2), POM-particulate org matter (=1.40×organic carbon), BC-black carbon
[+] 2.5% of sulfur should be emitted as particulate SO_2, most sulfur (S) is emitted as gaseous SO_2
[H] 0–100 m, 100–500 m, 500–1000 m, 1–2 km, 2–3 km, 3–6 km, assignment according to Table 4
[A] Cooke et al. (1999) report a more moderate amount of 10.1 Tg OC-C/yr.
[B] based on EDGAR3.2 FT2000 (http://www.rivm.nl/edgar) and Olivier et al. (2005)

Table 4. Fractional distribution (in %) of emission heights for wild-land fires.

	0–100 m *	100–500 m	500–1000 m	1000–2000 m	2000–3000 m	3000–6000 m
agricultural waste	100	–	–	–	–	–
tropical (30 S–30 N)	20	40	40	–	–	–
Temperate (30 N–60 N, 30 S–60 S)	20	20	20	40	–	–
Boreal (Eurasia)	10	10	20	20	40	–
Boreal (Canada)	10	10	10	10	20	40

* contributions assigned to heights below the actual altitude are moved into the lowest applicable height range and contribution of the 0–100 m altitude are always emitted in the lowest modeling layer.
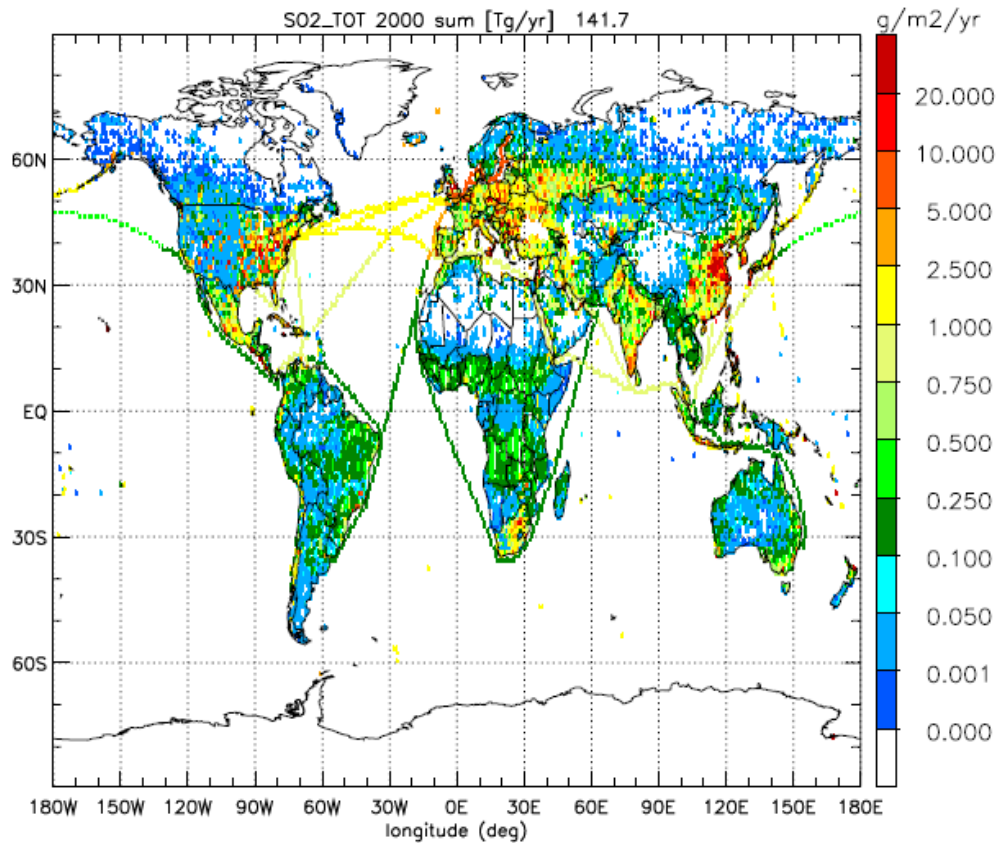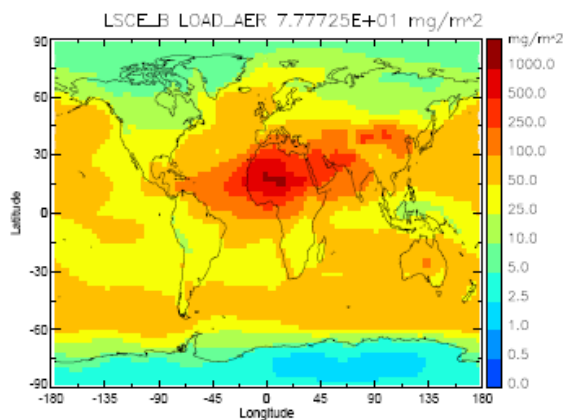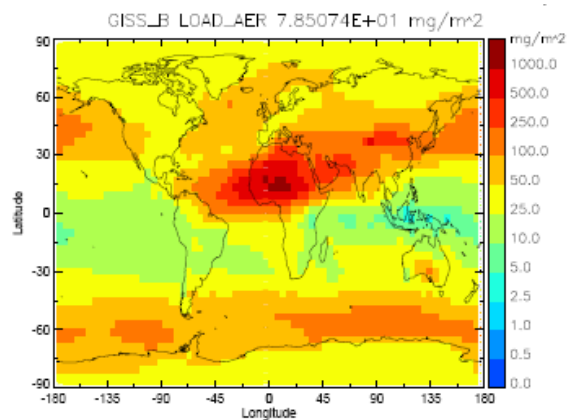
Fig. B4. Global distribution of all SO$_2$ emissions for the year 2000.

2. Compile the source code
3. Prepare the running script
4. Submit the job
5. Comparing results with other models and observations

GISS_B LOAD_AER 7.85074E+01 mg/m^2

LSCE_B LOAD_AER 7.77725E+01 mg/m^2

d)

MOZGN_B LOAD_AER 8.35446E+01 mg/m^2

UIO_CTM_B LOAD_AER 7.03477E+01 mg/m^2